Operando X-ray absorption spectroscopy of WO_3 photoanodes

Martina Fracchia,[1] Vito Cristino,[2] Alberto Vertova,[3,4] Sandra Rondinini,[3,4] Stefano Caramori,[2] Paolo Ghigna,[1,4] Alessandro Minguzzi[*,3,4]

[1] Dipartimento di Chimica, Università degli Studi di Pavia, Viale Taramelli 13, 27100 Pavia, Italy

[2] Dipartimento di Scienze Chimiche e Farmaceutiche, Università degli Studi di Ferrara, Via Luigi Borsari 46, 44121, Ferrara, Italy

[3] Dipartimento di Chimica, Università degli Studi di Milano, Via Golgi 19, 20133 Milano, Italy

[4] Istituto Nazionale di Scienza e Tecnologia dei Materiali, via Giusti 9, 50121, Firenze, Italy

* Corresponding Author. alessandro.minguzzi@unimi.it

Abstract

In this work we demonstrate the feasibility of hard X-rays operando XAS in photoelectrochemistry. WO_3, one of the most studied photoanodes for water splitting and for environmental remediation, is here studied at the W L_{III}-edge. This guarantees the direct observation of the W 5*d* band.

The material, that is preliminary fully characterized in terms of its photoelectrochemical features, is studied in a three-electrode spectroelectrochemical cell, while X-ray absorption is measured in the X-ray absorption near edge structure (XANES) region.

The recording of differential spectra and the monitoring of X-ray absorption at constant energy are used to compensate for the little XANES differences expected in the dark and under visible light illumination, which otherwise risks to be masked by experimental errors and/or after signal manipulation for data analysis.

The results point to the filling of the W t_{2g} orbitals under illumination, that is followed by a structural rearrangement that compensates for the accumulation of electrons in the conduction band under open circuit (OC) conditions.

Keywords: photoelectrochemistry, spectroelectrochemistry, water splitting, XANES, FEXRAV, tungsten oxide.

1. Introduction

The need for the efficient exploitation of renewable energy sources calls for the development of suitable energy conversion devices. In particular, solar energy harvesting requires the use of an energy vector capable of storing sunlight energy to compensate its intermittent nature. H_2 is the best candidate to this role, and photoelectrochemical water splitting (PEC-WS) guarantees the production of high purity H_2.

In PEC-WS, a semiconductor immersed in solution and coupled to a counter-electrode is illuminated by solar light. Light absorption by the semiconductor causes the formation of electron/hole pairs, which are separated and can drive two half-reactions thanks to the electrical field generated within the semiconductor at the semiconductor/liquid junction (SCLJ). Quite often, this requires the help of an external applied potential (bias). For n-type semiconductors, the anodic reaction (that proceeds by the transfer of holes to water) occurs at the semiconductor surface while the cathodic reaction is driven at the counter-electrode.

In the case of water splitting, the anodic process is the oxygen evolution reaction (OER):

$$2H_2O \rightarrow 4e^- + 4H^+ + O_2 \qquad (1)$$

That is a complicated reaction due to the need of exchange 4 electrons for each O_2 molecule.

In addition, electron-hole recombination, either in the bulk of the semiconductor or at surface defects represents the major parasitic phenomenon limiting the solar-to-hydrogen efficiency.

Several methods for better understanding the physical-chemistry of the SCLJ have been proposed so far[1], starting from the analysis of photocurrent transients to time-resolved absorption spectroscopy[2]. X-ray absorption spectroscopy (XAS) represents a powerful tool in that allows determining the oxidation state and the chemical surrounding of an absorbing atom. Moreover, XAS deals with the excitation of core (non-valence) electrons: this is key to make the technique element selective.

XAS is a bulk technique, as hard X-rays have a penetration depth of the order of microns. This represents a major drawback in studying interphases, since XAS averages the properties of all absorbing atoms within the X-ray beam. Notwithstanding this, operando XAS in electrochemistry proved to be effective in probing absorption phenomena and in determining the nature of active sites in inner sphere reactions[3][4][5]. In photoelectrochemistry, the use of operando XAS is quite scarce[6], being limited to a poor number of studies, i.e. of hematite photoanodes[7] and of relevant overlayers. In the latter case, the operando experiment involved the detection of any XAS spectral change of the overlayer (IrO_x, thus at the Ir L_{III} edge) while the semiconductor was in the dark or illuminated[8][9]. This limited number of papers is likely due to (i) the limited access to synchrotrons and (ii) to the difficulty in detecting, with significant statistics, the subtle spectral differences between

a photoelectrode in the dark and under illumination. In fact, together with the aforementioned limit of surface selectivity (where photogenerated charges might accumulated and be detected), recombination strongly limits the number of long-living photogenerated charges. Indeed, while short-living charges can be detected by ultrafast time resolved XAS, this has never been realized under operative, photoelectrochemical conditions.

We foresee two possible solutions. The first one deals with the *ad-hoc* preparation of a sample with a very high surface-to-bulk ratio. In this way, charges stored at the interface could be better detected. However, this kind of sample likely represents a poor performant photoelectrode and the "operando" conditions are not fully satisfied. The second option consists in carrying out specific XAS techniques for direct comparing "dark" and "light" conditions, making minor changes (in the order of a few percent in the absorption coefficient, μ) well evident above the experimental error.

In this work, we implement the second strategy for the operando study of WO_3, one of the most studied and promising n-type semiconductors for PEC-WS. We developed two complementary methods:

1) The acquisition of differential spectra $\Delta\mu$: for each X-ray photon energy the acquisition was performed both under visible light and in the dark to minimize possible systematic errors. This ensures that for each energy value the absorption coefficient under light and dark conditions is measured under the same instrumental conditions and can be directly subtracted.

2) The X-ray energy is kept constant, at values corresponding to the highest contrasts between the absorption coefficient of different standards phases. Obviously, this implies to record spectra of standard materials. This approach is similar to the one that we adopted for FEXRAV (fixed energy X-ray absorption spectroscopy)[10–12] where, under operative conditions and during the acquisition of the absorption coefficient, the electrode potential is varied at will. In the case of photoelectrochemical phenomena, this approach can be used to immediately compare the absorption coefficient under light and in the dark, recording the photocurrent and the spectroscopic information in sync, without the need of any data treatment.

As model system, we chose WO_3, one of the most studied visible absorbing n-type semiconductor to be used as photoanode for water splitting and for wastewater remediation.[13]

Moreover, X-ray absorption at the W L_{III}-edge (10.204 keV) implies the excitation, in the X-ray absorption near edge structure (XANES) region, of 2*p* to 5*d* orbitals. This reflects on the possibility of a direct observation of the occupancy of the 5*d* band of W.

In this work, we show that operando XAS for the study of an SCLJ is feasible and that it allows the direct observation of the semiconductor bands under working conditions.

2. Experimental

2.1 Preparation of WO_3 photoanodes

H_2WO_4 was generated from 2.5 g of Na_2WO_4 (AlfaAesar) by addition of 20 ml of concentrated HCl (Aldrich), followed by several washings in order to eliminate NaCl. The colloidal suspension of H_2WO was obtained by addition of 2 g of oxalic acid (Aldrich) at 60 °C. Transparent nanocrystalline electrodes cast onto well cleaned FTO (Pilkington TEC 7) glass were prepared by sequential spin coating deposition of the H_2WO_4 precursor prepared by adding 20% w/w Carbowax (Aldrich, 15000–20000 u) and triton X-100 (Fluka) (1 drop/2 g of colloidal precursor) to the H_2WO_4/oxalic acid colloid [21]. After each deposition the electrode was heated at 550°C for 30 min in air. Up to six spin coated layers afforded nanocrystalline electrodes having a thickness of ca. 1.5 µm. All electrodes have geometrical active area of 1 cm^2.

2.2 Photoelectrochemical and Electrochemical measurements.

Linear sweep voltammetry (LSV) curves of the WO_3 photoanodes under solar simulated illumination (ABET AM 1.5 G) were recorded with an Autolab PGSTAT 302/N in a three electrode cell containing 0.5 M Na_2SO_4, at a scan rate of 20 mV/s in the -0.2/1.5 V *vs.* SCE interval. Shuttered curves were obtained by manually shutting the illumination source. Photovoltage measurements were performed by zero current chronopotentiometry by preconditioning the photoanode at 300 mV *vs.* SCE for 180 s. The photovoltage relaxation with time, following restoration of the dark conditions was fitted with a biexponential function (1) in to extract the relative time constants

$$y = y_0 + A_1 e^{-x/t_1} + A_2 e^{-x/t_2} \qquad (1)$$

Incident photon to current efficiency (IPCE) spectra were collected with a previously described apparatus and [14] under constant 1.5 V *vs.* SCE bias. Uv-Vis spectra were obtained in transmission mode with a JASCO UV-570 spectrophotometer.

Cyclic voltammetry was recorded with scan speeds ranging from 10 mV/s to 100 mV/s between -0.2/1.5 V *vs.* SCE in the dark.

In the following data presentation and discussion all measured potentials vs SCE, were converted to the RHE scale.

2.3 Operando XAS. X-ray Absorption Spectra at the W-L_{III} edge were acquired in the fluorescence mode at the LISA beamline [http://www.esrf.eu/UsersAndScience/Experiments/CRG/BM08] at ESFR (European Synchrotron Radiation Facility), using a Si(311) double crystal monochromator, Pd mirrors with a cut-off energy of 20 keV for the harmonic rejection and a 13-element Ge fluorescence detector. The energy calibration was performed by measuring the Absorption Spectrum of a metallic W foil at the W-L_{III} edge. Spectra of reference samples (powders) were acquired in the transmission mode and used as standards. For those measurements, a proper amount of sample (to give a unit jump in the absorption coefficient) was mixed with cellulose and pressed into a pellet.

All data were obtained at room temperature. $\Delta\mu$ spectra (light minus dark) were obtained by collecting the W L_{III}-edge XANES in UV-Vis in light and dark conditions and in parallel: for each energy value, the acquisition was performed both in presence and in absence of UV-Vis illumination before moving to higher energy values in order to minimize systematic errors. The acquisition time for each point was set to 10 s. In order to check for possible sources of spurious signals in $\Delta\mu$, due to casual variations in the fluorescence yield, each of the $\Delta\mu$ data collection was repeated at least 3 times, obtaining the same results above the noise level for each of the repetitions.

The UV-Vis illumination was achieved by means of a 400 nm LED.

The LED light is focused at the back of the photoelectrode. The latter is lodged in a spectroelectrochemical cell, filled with 0.1 M aqueous Na_2SO_4 (in Milli-Q grade water) with a three-electrodes configuration, using a AgCl/Ag (1M KCl) and a Pt wire as reference and counter electrode, respectively.

The electrode potential is controlled by a CH Instruments 633d potentiostat.

The cell is made of a silicon rubber structure that holds two plastic walls transparent to visible light. The window in front of the working electrodes is made of thin Mylar® foil to guarantee a low X-ray absorption.

X-ray signal extraction and normalization was performed by means of the ATHENA code, belonging to the set of interactive programs IFEFFIT [15,16]. The pre-edge back ground was fitted by means of a straight line and the post edge back ground by means of a cubic spline. At each of the stationary potentials investigated in this work, ($\Delta\mu$, light-dark) spectra were obtained first by normalizing each of the spectra in dark and light condition at unit absorption at *ca.* 200 eV after the edge, and then by subtracting the normalised dark spectrum from the analogous spectrum in light conditions.

3. Results and discussion

3.1General Photoelectrochemical Properties

Figure 1 shows the absorption spectrum of the transparent WO_3 films extending up to 460 nm, with the absorption increasing towards UV wavelengths. The indirect band gap, using the Tauc analysis employing IPCE data (to avoid optical interference effects of the thin film) is 2.58 eV, consistent with the 2.6 eV reported for monoclinic WO_3 [17][18].

The morphology of these mesoporous films has been reported in various previous contributions, and AFM and SEM microscopies have shown them to consist in a network of roughly spherical nanoparticles having *ca.* 50 nm diameter assembled in a film with a thickness of 1.5±0.2 μm [14,19,20].

A typical LSV curve recorded under solar simulated illumination is reported in **Figure 2** and is consistent with the typical behaviour of an n-type electrolyte junction with the photoanodic current rising with increasing anodic potential. The photocurrent onset occurs at *ca.* 0.75 V *vs.* RHE while the limiting photocurrent, which corresponds to the maximum hole transfer rate to the electrolyte, is observed for V > 1.7 V *vs*. RHE. In neutral sodium sulfate, hole transfer results in the oxidation of both water to dioxygen and of sulfate anions to persulfate, with the second hole scavenging pathway dominating over the first [21]. In the entire anodic scan range, from 0.75 V *vs.* RHE onwards, the dark contribution (blue line) to the current is negligible, as confirmed by the good match of the steady state curve with the photocurrent transients obtained by chopping the light source. The IPCE spectrum, **Figure 2** (right) is consistent with the absorption spectrum, showing the photoconversion onset at 460 nm. The photoconversion maximum of 45 % is reached at *ca.* 350 nm, followed by a decrease due to the cell optical glass transmission. Given that the light harvesting efficiency (LHE) approaches unity at 350 nm, and that $IPCE(\lambda) = \varphi_{e/h}\eta_{tr}\eta_{interface}LHE(\lambda)$ with unitary $\varphi_{e/h}$ (quantum yield of electron and hole generation) we can conclude that the maximum IPCE is determined by the product $\eta_{tr}\eta_{interface}$, which contains the hole transport efficiency from the semiconductor to the interface (η_{tr}) and the scavenging efficiency $\eta_{interface}$. Since in the presence of organic hole scavengers like methanol or formic acid the IPCE of these WO_3 films reaches or even exceeds 100 % [22], we can conclude that interfacial hole transfer is the rate limiting step, rather than transport.

The chronopotentiometric experiment reported in **Figure 3** top, is helpful for evaluating the flat band potential and the existence of long-living charge trapping phenomena. During the experiment, the electrode is first anodically polarized at a potential where no faradaic processes are observed (*i.e.* ≥ 0.95 V *vs.* RHE), then held in the dark while measuring the open circuit potential (OCP) until the

achievement of an almost steady potential; illumination is finally switched on after 300 s from the beginning of the experiment. As soon as illumination is on, a sudden drop of the potential towards less positive values occurs as photogenerated holes are scavenged (at least partially) by the electrolyte (either water or SO_4^{2-} ions), while electrons accumulate in the solid under open circuit conditions. A first 150 mV drop between 0.75 and 0.6 V happens in *ca.* 7 s, followed by slower 30 mV drift in *ca.* 170 s. At the end of the illumination step, the negative drift is not yet completed, suggesting that a slow and progressive filling of states continues to occur under steady illumination. As this drift is small, in the range of few mV, a reasonable estimate of the flat band value of WO_3 can still be obtained from the photovoltage plateau attained under illumination. The value of *ca.* 570 mV *vs.* RHE can be therefore assumed as a good figure. The voltage recovery due to charge recombination in dark conditions is extremely slow and clearly multiexponential with at least two lifetimes, one of the order of 50 seconds, and the other one of 460 s: these lifetimes have only a qualitative meaning, given that the recombination kinetic is far from being complete after 1000 s.

The multiexponential kinetics is symptomatic of multiple electron recombination pathways which can involve reaction with surviving holes, scavenging by oxygen (a very slow process with WO_3) [23], reaction with oxidant species like persulfate and hydrogen peroxide generated by hole injection into the electrolyte during the light cycle. With the exception of the electron-hole recombination in the bulk of the solid, the other electron recapture events are generally slow bimolecular multi-electron processes, allowing for the persistence of an excess of negative charge stored within the mesoporous film for at least several hundred seconds. Charge compensation thus occurs by means of a cation flux from the electrolyte into the mesoporous network. Cyclic voltammetry in the dark, **Figure 3** bottom, reveals clear diffusion controlled waves centred at *ca.* 0.55 V *vs.* RHE, in good agreement with the flat band estimate from the photovoltage study. This process corresponds to injection of electrons into empty states of the semiconductor accompanied by the diffusion of ions from the electrolyte.

3.2 Operando XAS

Figure 4 reports a pictorial scheme for the spectroelectrochemical cell used for this work. It consists of a pouch with polyethylene terephtalate walls separated by silicon spacers. The working electrode is back illuminated by a 5 mW 400 nm LED. In front of the sample, a thin Mylar® window (10 μm) is glued in order to minimize undesired X-ray absorption by the cell.

The volume of the electrolyte in front of the sample is controlled by using parafilm® spacers at the back of the electrode, to minimize X-ray absorption by the electrolyte solution while avoiding excessive ohmic drop contributions. Four spacers (about 2x2 mm^2 each) are stuck onto the electrode back at the four corners before immersion in the electrolyte.

The choice of a high power LED comes from the need of increasing the rate of photocarriers generation, to enhance their effect in the XAS spectra.

Figure 4 reflects the choice of this experimental setups in terms of a cyclic voltammetry recorded at 20 mV s^{-1} on a WO_3 photoanode in the dark and under 400 nm LED illumination. These curves were recorded in the described spectroelectrochemical cell and in the experimental XAS hutch, before the recording of a XAS spectra. Here two different electrodes belonging to same preparative batch are compared. The one measured in the beaker cell was actually one of those used during XAS experiments, whose J/E was measured to confirm photoanode stability following repeated spectroelectrochemical experiments.

Although slight variations in photoelectrode response are possible, depending on sample preparation and, more importantly on photoelectrode history (i.e. previous illumination and polarization cycles), we can observe that the photoanodic onset, one of the main relevant figures for our operando experiments, are practically coincidental in both cell configurations. The higher IR drop in the XAS photoelectrochemical cell, expected given the cell design with larger inter-electrode distance, results however in a more rectilinear shape (ohmic behavior) of the photocurrent/voltage characteristics, leading to lower slope of the J/E curve. Nevertheless, despite a degradation of the J/E characteristics, the magnitude of the photocurrent in the XAS cell is, for equivalent voltages out to 1.2-1.3 V vs NHE, still fully comparable to that of the conventional cell. It should be recalled that in order to limit bubble formation under illumination, we limited the applied potential to 1.3 V. Within this potential interval, the similarity between the amount of carriers generated and extracted from the semiconductor/electrolyte junction in both cells, allows to validate and extend our spectroscopic results also to other working conditions where cells with better iR drop characteristics can be conveniently used.

Figure 5, left panel, shows the W L_{III}-edge spectra of WO_3 as it is, after annealing in air for 1 h at 900 °C, after reduction in a flux of gaseous NH_3 at 900 °C for 12 h, and of a sodium tungsten bronze. The white line (WL) in WO_3 presents a typical spectral shape, due to transition from the W 2*p* states to empty 5*d* states split by the crystal field in states with t_{2g} and e_g symmetry[24], as better shown in the inset of Fig. 5. Heating in air at 900 °C causes a marked increase in the WL intensity, probably related with changes in the local distortions of the WO_6 octahedra [25,26]. Reduction of W by NH_3, or by producing a sodium tungsten bronze, causes the WL to shift toward lower energy. This is the XAS chemical shift and is due to the different screening of the core level by outer (valence) electrons. The shift is better evidenced by plotting the first derivative of the spectra, as it is shown in the right panel of **Figure 5**.

For what concerns the intensity of the WL, it is noted that the differences in **Figure 5** are large, and again probably related to different local structures. It is also observed that the WL intensity is very sensitive to minor changes in the local distortions. Indeed, as it is shown in **Figure 6** (left upper panel) the spectrum of the electrode material when immersed in the electrolytic solution shows a marked *increase* in the intensity of the white line. When an anodic potential is applied (1.1V **Figure 6**, left bottom panel, black dashed line), the overall spectral shape is unchanged as expected since W(VI) cannot be oxidised further. Upon the application of a potential lower than the OCP, 0.35 V (**Figure 6** lower panel, green curve), the WL intensity is largely increased, which may be symptomatic of the formation of a sub-stoichiometric WO_{3-x} phase and/or of the Na^+ intercalation in the WO_3 structure, with the formation of a sodium tungsten bronze. This suggestion is somewhat confirmed by the fact that a second spectrum taken after keeping the electrode at the same potential for 2 h (blue curve) shows a decrease in the intensity of the white line. This indicates a slower kinetic second phenomenon is underway, that is in turn compatible with the diffusion of Na^+ ions inside (or OH^- outside) the WO_3 structure as the rate determining step.

The behaviour of WO_3 as photoelectrocatalyst was also studied by in situ XAS at the W L_{III}-edge, in OCP conditions, and under a potential where photocurrents are not observed (0.35 V) and at a higher potential, where photocurrents are observed but bubble formation is not negatively affecting the XAS signal-to-noise ratio (1.1 V). Results are shown in **Figure 7**, as $\Delta\mu$ spectra obtained as described in the experimental. Some preliminary considerations concerning the noise level in the $\Delta\mu$ spectra are worth of mention here. First, we note that subtracting two spectra results in summing the noise of both. Second, we note that the $\Delta\mu$ technique is indeed a powerful tool for extracting small differences between two XAS spectra obtained in different experimental conditions; therefore, the $\Delta\mu$ spectra are expected to give quite small signals. As a matter of fact, a sensible estimate of the number of W centers involved in the UV-Vis photoexcitation process can be obtained by assuming that: i) the excitation power has a sensible figure of 0.1 W/cm^2 at 400 nm; ii) the film is formed of spherical particles with an average diameter of 50 nm for a total thickness of 1.5 μm; and iii) each nanoparticle is formed by WO_6 octahedra having a spherical footprint with a radius given by the WO distance. This would give a figure of about 1/100 of the centers of W in the film that are excited, contributing for an electron.

That said, it is apparent in **Figure 7** that differences above the unavoidable noise level are obtained only in OCP conditions. This may be due to the fact that, upon applying a potential, photogenerated electrons are rapidly swept from the electrode and transferred to the counter electrode through the external circuit. Under OCP conditions, it should also be noted that: i) the $\Delta\mu$ spectrum is significantly negative in correspondence to the t_{2g} orbitals only, and it is negligible in correspondence of the e_g

orbitals. As the WL intensity reflects the density of the final empty states, a negative $\Delta\mu$ is due to the filling of the conduction band by photoexcitation from the valence band (see **Figure 6** right panel); ii) the $\Delta\mu$ spectrum shows only part(s) of a more complicated phenomenon that takes place with a very slow kinetics. We first note that direct photoexcitation to the eg orbitals would require at least 6 eV, and therefore cannot be obtained by illuminating with our LED that has an energy of 3 eV only. Second, pump and probe experiments by Uemura and co-workers [27,28] pointed out that on dispersed WO_3 nanoparticles, the $\Delta\mu$ shows a difference at both the t_{2g} and e_g orbitals; however, they also pointed out that the difference close to e_g energy is due to a structural rearrangement of WO_3 rather than to the photoexcitation process. It should be noted that the timescale of the phenomena investigated by Uemura et al. is very short (hundreds of ps), and therefore it is not surprising that we could not detect an identical behaviour by performing quasi steady-state experiments probing a time average of the different phenomena taking place in the sample. It is also noted that the amplitude of the $\Delta\mu$ signal at OCP is in nice agreement with the estimate given above.

For a better understanding of this complex behaviour we performed measurements of the X-ray absorption coefficient at fixed energy by alternating periods of light and dark condition. The results are shown in **Figure 8**, where open circuit potential profiles match those reported in **Figure 3** reaching about 0.55 V under illumination and about 0.70V in the dark, with a faster progressive drift towards more positive dark OCP values (from 0.68 to 0. 72 V vs RHE) as the number of illumination cycles increases. It is worth to mention that the Fermi level in the dark during water splitting experiments is not well defined, lacking the presence of a kinetically fast redox couple in precise concentration in the electrolyte. The relevant redox couple initially present in the electrolyte is here represented by the O_2/H_2O couple, but other redox couples, like $S_2O_8^{2-}/SO_4^{2-}$ and H_2O_2/H_2O are generated during photoanode operation, besides a local concentration of protons as a result of water oxidation. Spectroelectrochemical cell constrictivity effects will eventually slow down the electrolyte mixing, compared to a conventional electrochemical cell, exacerbating the local accumulation of these species in the proximity of the photoanode. Since electron acceptors ($S_2O_8^{2-}$, H_2O_2, O_2) and potential determining ions (H_3O^+) are created and accumulated at photoanode/electrolyte interface during illumination cycles, we expect that indeed these species will contribute to stabilize (i.e. positively shift) the Fermi level of WO_3 in the dark while leading to a kinetically faster relaxation of the photovoltage once dark conditions are established, due to redox mediated electron recapture. Light and dark states are reproducibly associated to changes of the absorption coefficient: in correspondence of the t_{2g} energy, when the light is switched on, μ has a sharp decrease due to the injection of the electrons in these states, followed by a slow increase to a steady value. In addition, the value of μ in stationary conditions increases after each light/dark cycle. On the contrary, the same

plot at the e_g energy shows only the increasing trend, thus demonstrating that no direct injection occurs in these orbitals. This is in agreement with the $\Delta\mu$ spectra reported in **Figure 7** (OCP), which refers to the initial 10 s that follow every illumination or dark step.

In conclusion, these results demonstrate the presence of some processes, likely related to some structural rearrangements in the electrode, that take place on a very long timescale, which would be out of reach by pump and probe experiments. It is quite reasonable to associate these structural changes with the ionic flux towards or outwards the current collector.

A final comment is due concerning the fact that the negative peak in $\Delta\mu$ is observed at *ca.* 2 eV below the actual energy of the t_{2g} orbitals. To explain this fact, we first note that the natural width of the W L_{III}-edge is ca. 5 eV, and therefore all the spectral features detected at this edge are at least affected by such a broadening; second, the WO_3 band gap is 2.58 eV, while the width of the t_{2g} band is at least 2 eV, meaning that by illuminating with UV-vis photons at 400 nm (3 eV), only low lying states at the bottom of the t_{2g} band can be reached. The combination of these two factors is possibly at the origin of the observed shift.

4. Conclusions

This paper demonstrates the possibility of operando X-ray absorption spectroscopy for the study of photoelectrodes. The term "operando" was adopted in that the experimental conditions are as close as possible (in terms of presence of the electrolyte, use of a three-electrode cell and illumination with visible light) as those normally adopted for a photoelectrode characterization.

In order to overcome the main hindrance to the effectiveness of this approach, differential spectra acquisition and constant energy absorption coefficient determination were adopted. The results, compared with the spectra collected on standard samples, lead to new insights on the semiconductor-electrolyte junction. Spectra were recorded at the W L_{III}-edge, to have a direct access to the W *d* states in the conduction band.

Here we show that, in the case of a WO_3 photoelectrode in contact with a Na_2SO_4 aqueous solution, at the OCP and under illumination, two parallel (and most likely correlated) phenomena occur:

1. a structural change, which increases the intensity of the XANES peak.
2. the filling of the t_{2g} W orbitals, which lowers the XANES peak and is due to the photogeneration of electrons to the conduction band.

While the second one prevails at short times (within the first tens of seconds) the first is predominant in the entire XANES and particularly at high times.

A possible interpretation is that photogenerated electrons partially fill the W t_{2g} orbitals, and progressively drive a solid state redox transition that reflects in a structural rearrangement of the photoanode.

Under applied potentials, either lower or higher than the open circuit one, these changes become negligible, likely due to the effect of an applied potential, which drains photogenerated electrons and holes towards the solution/current collector.

5. Acknowledgements

We thankfully acknowledge beamline BM08 “LISA” at the European Synchrotron Radiation Facility for provision of beamtime (experiment 08-01-1004) and Francesco D’Acapito for the kind support during the experiment. Università degli Studi di Milano by the “Piano di Sostegno alla Ricerca” and Emilia Romagna Region by the S POR-FESR HP Solar Project are gratefully acknowledged for financial support.

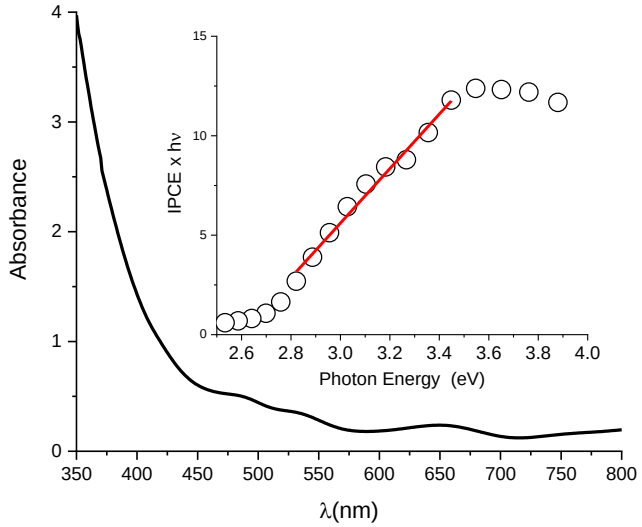

Figure 1. Absorption Spectrum of WO_3 thin film on FTO electrode. Inset: Tauc plot using IPCE data.

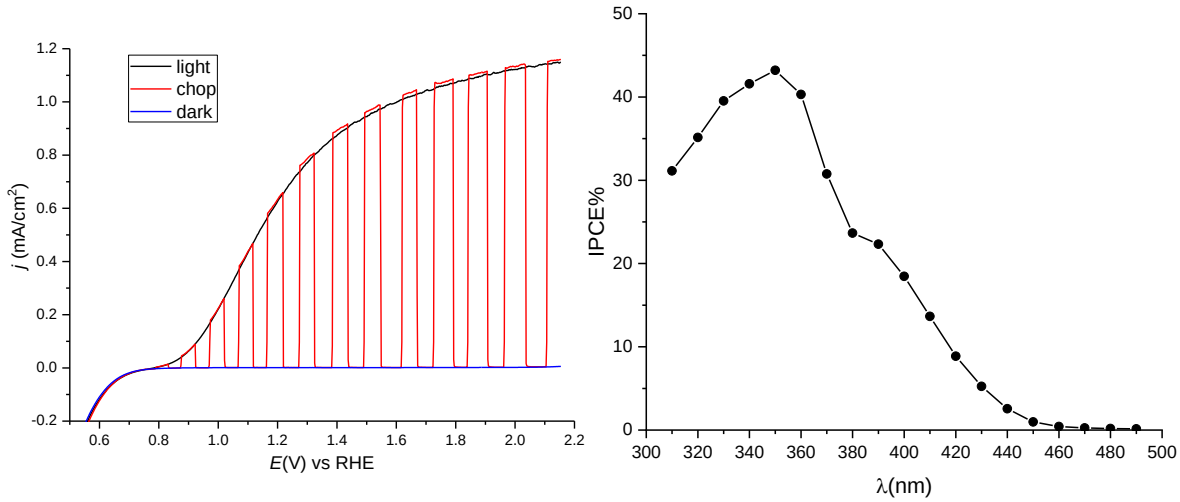

Figure 2 Left: JV curves of WO_3 in 0.5 M Na_2SO_4 under AM 1.5 G (black), in the dark, (blue) and under shuttered illumination (red); right IPCE under constant 2.15 V vs RHE.

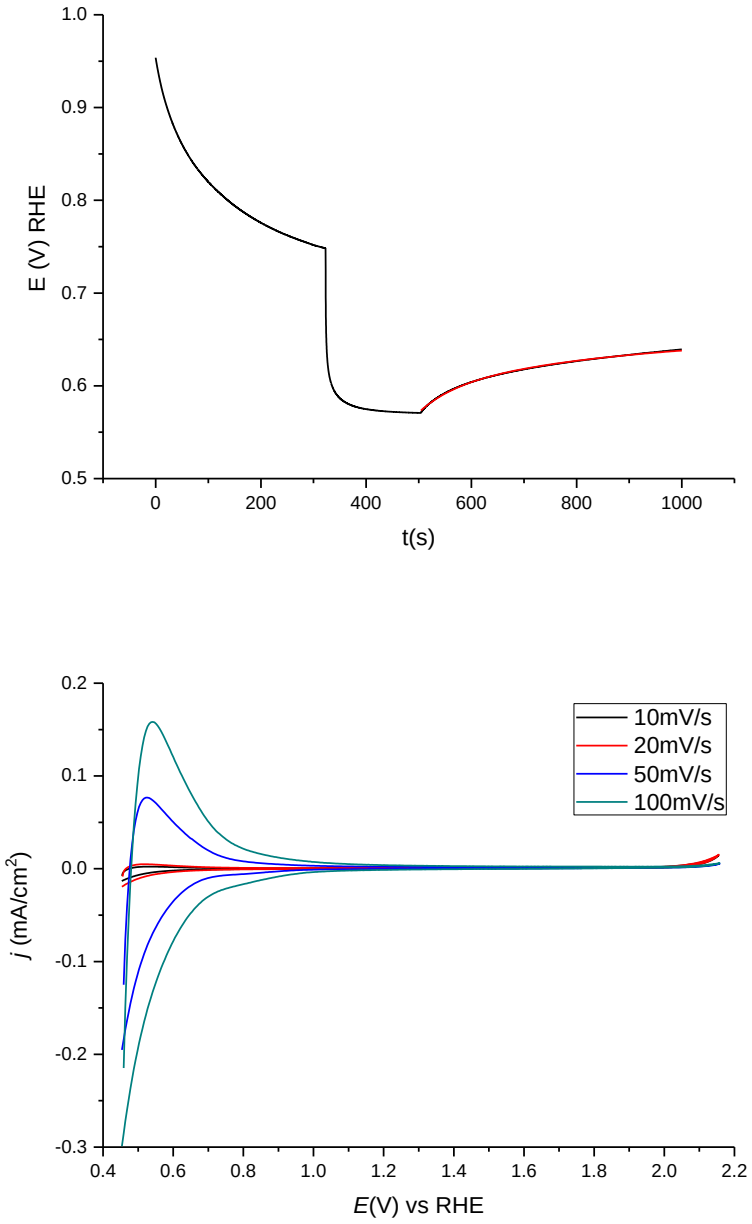

Figure 3 Top: WO_3 photovoltage generation and decay under open circuit conditions in 0.5 M Na_2SO_4 under AM 1.5 G; Bottom:Cyclic voltammetry of the WO_3 film in Na_2SO_4 under dark conditions upon various scan rates.

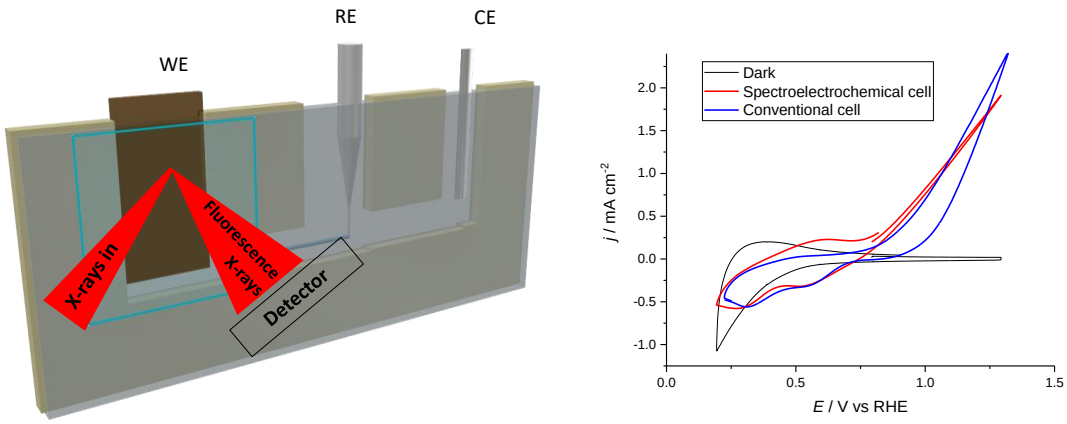

Figure 4. left panel: pictorial scheme of the spectroelectrochemical cell. The light blue square represents the Mylar window. Right panel: Cyclic voltammetry of WO_3 in 0.1 M Na_2SO_4 in the dark (black) and under 400 nm LED light in the spectrochemical cell (red) or in a quartz beaker (blue).

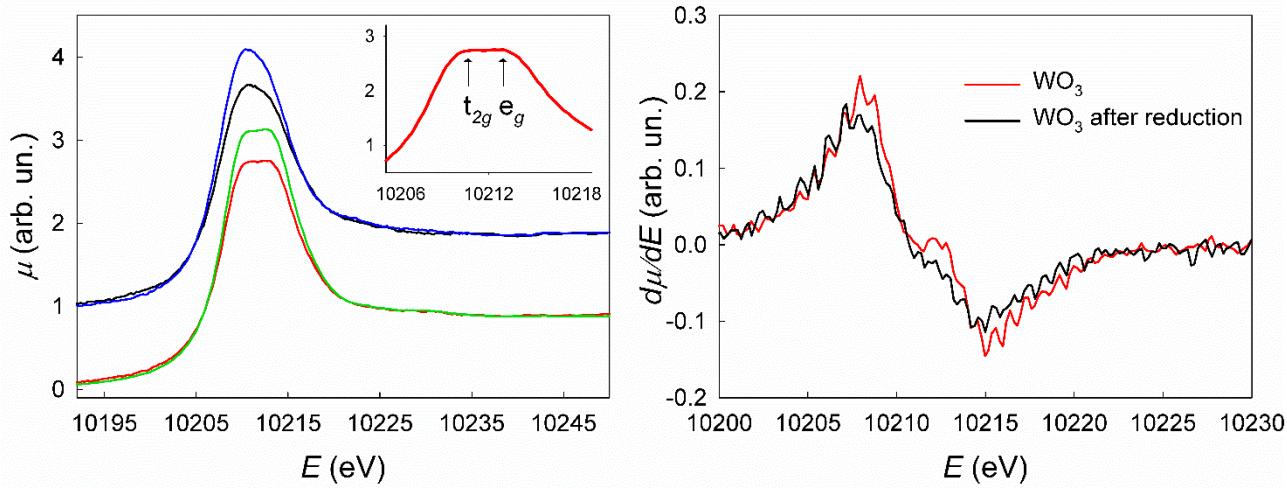

Figure 5. left panel: W L_{III}-edge XANES spectra of WO_3 (red line), of WO_3 after annealing in air for 1 h at 900 °C (green line), of WO_3 after reduction in a flux of gaseous NH_3 at 900 °C for 12 h (black line) and of a tungsten bronze (blue line). The spectra are shifted along the *y* axis for the sake of better clarity. Right panel: 1st derivative spectra of WO_3 (red line) and WO_3 after reduction (black line).

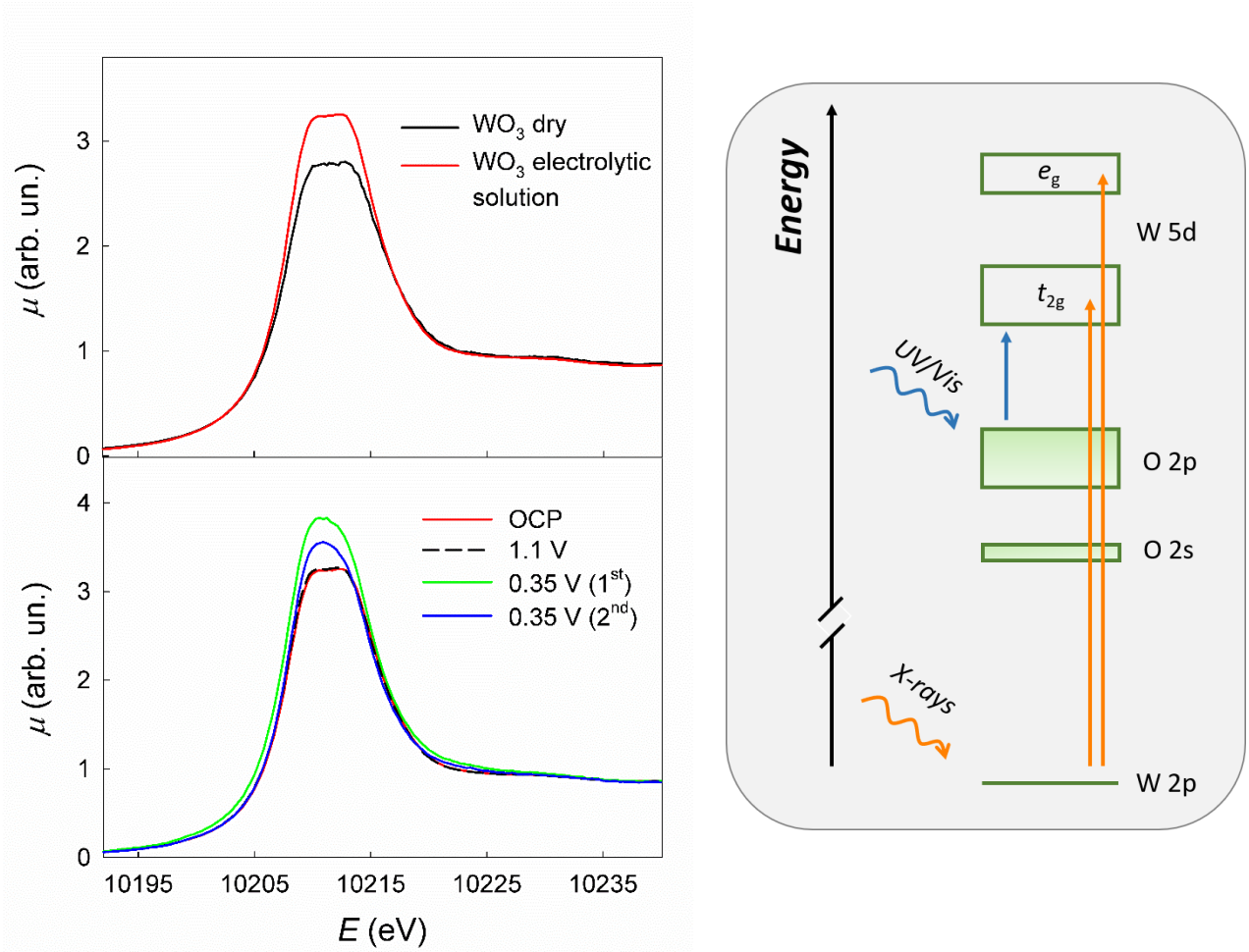

Fig. 6 upper left panel: W L_{III}-edge XANES spectra of WO_3 (red line), and of the WO_3 electrode immersed in the electrolytic solution (black line). Lower panel: W L_{III}-edge XANES spectra of the WO_3 electrode at OCP (red line), at 1.1 V (black dashed line), at 0.35 V (green line) and at the same potential but after 2h (blue line). On the right, a schematic of the band structure of WO_3 and of the electron excitations described in this work is shown.

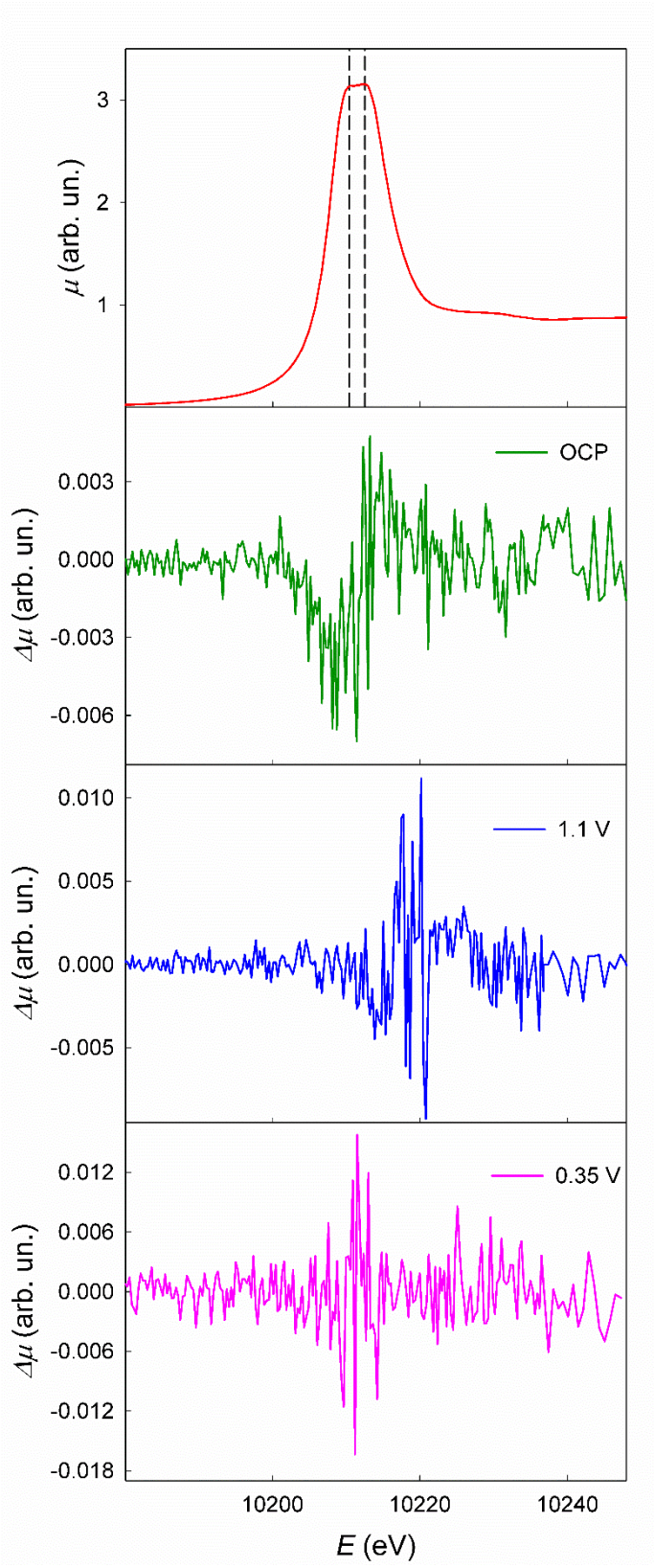

Figure 7. $\Delta\mu$ spectra at the W L_{III}-edge at OCP (green curve), 1.1 V (blue curve) and 0.35 V (magenta curve); the red curve in the upper panel shows the XANES W L_{III}-edge spectrum of WO_3 for better reference, where the dashed lines are in correspondence of the energy of the t_{2g} and e_g orbitals.

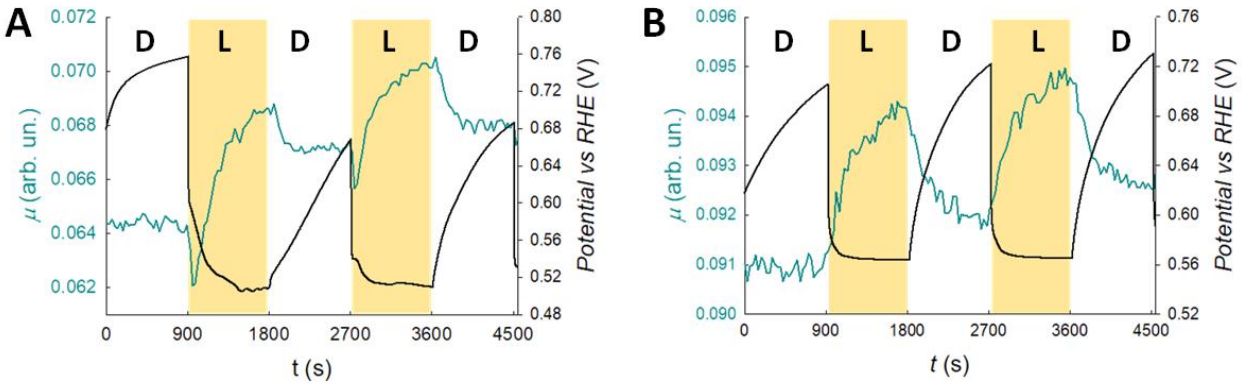

Figure 8. left, blue axis: Fixed energy X-ray absorption coefficient plotted as a function of time at the energy of the W t_{2g} (A, 10211 eV) and e_g orbitals (B, 10213 eV). Right, black axes: open circuit potential.

References

[1] Z. Chen, H.N. Dinh, E. Miller, Photoelectrochemical Water Splitting - Standards, Experimental Methods, and Protocols, 2013. doi:10.1021/jm101179e.

[2] B.H. Simpson, J. Rodríguez-López, Emerging techniques for the in situ analysis of reaction intermediates on photo-electrochemical interfaces, Anal. Methods. 7 (2015) 7029–7041. doi:10.1039/c5ay00503e.

[3] A. Minguzzi, P. Ghigna, X-ray absorption spectroscopy in electrochemistry from fundamentals to fixed energy X-ray absorption voltammetry, in: A.J. Bard, C.G. Zoski (Eds.), Electroanal. Chem. A Ser. Adv. Vol. 27, CRC Press - Taylor and Francis Group, USA, 2017: pp. 119–181. doi:10.1201/9781315270302.

[4] A.E. Russell, A. Rose, X-ray absorption spectroscopy of low temperature fuel cell catalysts, Chem. Rev. 104 (2004) 4613–4635.

[5] E. Fabbri, D.F. Abbott, M. Nachtegaal, T.J. Schmidt, Operando X-ray absorption spectroscopy: A powerful tool toward water splitting catalyst development, Curr. Opin. Electrochem. 5 (2017) 20–26. doi:10.1016/j.coelec.2017.08.009.

[6] P. Ghigna, S. Rondinini, M. Fracchia, A. Vertova, A. Minguzzi, Time-Resolved X-ray Absorption Spectroscopy in (Photo)Electrochemistry, Surfaces. 1 (2018) 138–150. doi:10.3390/surfaces1010011.

[7] A. Braun, K. Sivula, D.K. Bora, J. Zhu, L. Zhang, M. Grätzel, J. Guo, E.C. Constable, Direct observation of two electron holes in a hematite photoanode during photoelectrochemical water splitting, J. Phys. Chem. C. 116 (2012) 16870–16875. doi:10.1021/jp304254k.

[8] T. Baran, M. Fracchia, A. Vertova, E. Achilli, A. Naldoni, F. Malara, G. Rossi, S. Rondinini, P. Ghigna, A. Minguzzi, F. D'Acapito, Operando and Time-Resolved X-Ray Absorption Spectroscopy for the Study of Photoelectrode Architectures, Electrochim. Acta. 207 (2016). doi:10.1016/j.electacta.2016.04.153.

[9] A. Minguzzi, A. Naldoni, O. Lugaresi, E. Achilli, F. D'Acapito, F. Malara, C. Locatelli, A. Vertova, S. Rondinini, P. Ghigna, Observation of charge transfer cascades in α-Fe_2O_3/IrO_x photoanodes by operando X-ray absorption spectroscopy, Phys. Chem. Chem. Phys. 19 (2017) 5715–5720. doi:10.1039/C6CP08053G.

[10] A. Minguzzi, O. Lugaresi, C. Locatelli, S. Rondinini, F. D'Acapito, E. Achilli, P. Ghigna, Fixed energy X-ray absorption voltammetry, Anal. Chem. 85 (2013) 7009–7013.

doi:10.1021/ac401414v.

[11] S. Rondinini, O. Lugaresi, E. Achilli, C. Locatelli, A. Minguzzi, A. Vertova, P. Ghigna, C. Comninellis, Fixed Energy X-ray Absorption Voltammetry and Extended X-ray Absorption fine Structure of Ag nanoparticle electrodes, J. Electroanal. Chem. 766 (2016). doi:10.1016/j.jelechem.2016.01.039.

[12] G. Montegrossi, A. Giaccherini, E. Berretti, F. Di Benedetto, M. Innocenti, F. d'Acapito, A. Lavacchi, Computational Speciation Models: A Tool for the Interpretation of Spectroelectrochemistry for Catalytic Layers under Operative Conditions, J. Electrochem. Soc. 164 (2017) E3690–E3695. doi:10.1149/2.0711711jes.

[13] C.A. Bignozzi, S. Caramori, V. Cristino, R. Argazzi, L. Meda, A. Tacca, Nanostructured photoelectrodes based on WO3: Applications to photooxidation of aqueous electrolytes, Chem. Soc. Rev. 42 (2013) 2228–2246. doi:10.1039/c2cs35373c.

[14] V. Cristino, S. Marinello, A. Molinari, S. Caramori, S. Carli, R. Boaretto, R. Argazzi, L. Meda, C.A. Bignozzi, Some aspects of the charge transfer dynamics in nanostructured WO3 films, J. Mater. Chem. A. 4 (2016) 2995–3006. doi:10.1039/c5ta06887h.

[15] M. Newville, IFEFFIT : interactive XAFS analysis and FEFF fitting, J. Synchrotron Radiat. 8 (2001) 322–324.

[16] B. Ravel, M. Newville, ATHENA, ARTEMIS, HEPHAESTUS: data analysis for X-ray absorption spectroscopy using IFEFFIT, J. Synchrotron Radiat. 12 (2005) 537–541.

[17] L. Ottaviano, L. Lozzi, M. Passacantando, S. Santucci, On the spatially resolved electronic structure of polycrystalline WO3 films investigated with scanning tunneling spectroscopy, Surf. Sci. 475 (2001) 73–82. doi:10.1016/S0039-6028(00)01075-X.

[18] M. Gillet, K. Aguir, C. Lemire, E. Gillet, K. Schierbaum, The structure and electrical conductivity of vacuum-annealed WO3thin films, Thin Solid Films. 467 (2004) 239–246. doi:10.1016/j.tsf.2004.04.018.

[19] R. Argazzi, R. Boaretto, V. Cristino, M. Dal Colle, R. Bertoncello, S. Caramori, C. Stevanin, G. Longobucco, N. Marchetti, A. Molinari, C.A. Bignozzi, L. Pasti, A. Martucci, Photoelectrochemical degradation of pharmaceuticals at β25 modified WO3 interfaces, Catal. Today. (2018). doi:10.1016/j.cattod.2018.09.020.

[20] S. Caramori, N. Marchetti, R. Boaretto, A. Molinari, V. Cristino, G. Longobucco, C.A. Bignozzi, L. Pasti, Photoelectrochemical mineralization of emerging contaminants at porous WO 3 interfaces, Appl. Catal. B Environ. 204 (2016) 273–282. doi:10.1016/j.apcatb.2016.11.007.

[21] Q. Mi, A. Zhanaidarova, B.S. Brunschwig, H.B. Gray, N.S. Lewis, A quantitative assessment

of the competition between water and anion oxidation at WO3photoanodes in acidic aqueous electrolytes, Energy Environ. Sci. 5 (2012) 5694–5700. doi:10.1039/c2ee02929d.

[22] C. Santato, M. Ulmann, J. Augustynski, Photoelectrochemical Properties of Nanostructured Tungsten Trioxide Films, J. Phys. Chem. B. 105 (2001) 936–940. doi:10.1021/jp002232q.

[23] T. Suzuki, H. Watanabe, Y. Oaki, H. Imai, Tuning of photocatalytic reduction by conduction band engineering of semiconductor quantum dots with experimental evaluation of the band edge potential, Chem. Commun. 52 (2016) 6185–6188. doi:10.1039/c6cc01166g.

[24] S. Yamazoe, Y. Hitomi, T. Shishido, T. Tanaka, XAFS study of tungsten L1- And L3-edges: structural analysis of WO3 species loaded on TiO2 as a catalyst for photo-oxidation of NH3, J. Phys. Chem. C. 112 (2008) 6869–6879. doi:10.1021/jp711250f.

[25] J. Purans, E. Burattini, P. Cikmach, A. Lusis, E. Bernieri, A. Kuzmin, A. Balerna, XANES studies of MeO3-x (Me = W, Re, Ir) crystalline and amorphous oxides, Nucl. Instruments Methods Phys. Res. Sect. A Accel. Spectrometers, Detect. Assoc. Equip. 308 (2002) 240–242. doi:10.1016/0168-9002(91)90637-6.

[26] E. Oakton, G. Siddiqi, A. Fedorov, C. Copéret, Tungsten oxide by non-hydrolytic sol-gel: Effect of molecular precursor on morphology, phase and photocatalytic performance, New J. Chem. 40 (2016) 217–222. doi:10.1039/c5nj01973g.

[27] Y. Uemura, D. Kido, Y. Wakisaka, H. Uehara, T. Ohba, Y. Niwa, S. Nozawa, T. Sato, K. Ichiyanagi, R. Fukaya, S.I. Adachi, T. Katayama, T. Togashi, S. Owada, K. Ogawa, M. Yabashi, K. Hatada, S. Takakusagi, T. Yokoyama, B. Ohtani, K. Asakura, Dynamics of Photoelectrons and Structural Changes of Tungsten Trioxide Observed by Femtosecond Transient XAFS, Angew. Chemie - Int. Ed. 55 (2016) 1364–1367. doi:10.1002/anie.201509252.

[28] Y. Takagi, H. Wang, Y. Uemura, T. Nakamura, L. Yu, O. Sekizawa, T. Uruga, M. Tada, G. Samjeské, Y. Iwasawa, T. Yokoyama, In situ study of oxidation states of platinum nanoparticles on a polymer electrolyte fuel cell electrode by near ambient pressure hard X-ray photoelectron spectroscopy, Phys. Chem. Chem. Phys. 19 (2017) 6013–6021. doi:10.1039/C6CP06634H.